Endocrinology, 2023, **164**, 1–17
https://doi.org/10.1210/endocr/bqad022
Advance access publication 31 January 2023
Research Article

Evocalcet Rescues Secondary Hyperparathyroidism-driven Cortical Porosity in CKD Male Rats

Tomoka Hasegawa,[1] Shin Tokunaga,[2,3] Tomomaya Yamamoto,[1] Mariko Sakai,[3] Hiromi Hongo,[1] Takehisa Kawata,[2] and Norio Amizuka[1]

[1]Developmental Biology of Hard Tissue, Graduate School of Dental Medicine, and Faculty of Dental Medicine, Hokkaido University, Sapporo, Japan
[2]Medical Affairs Department, Kyowa Kirin Co., Ltd., Tokyo, Japan
[3]Biomedical Science Research Laboratories 1, Research Unit, R&D Division, Kyowa Kirin Co., Ltd., Shizuoka, Japan

Correspondence: Norio Amizuka, DDS, PhD, Developmental Biology of Hard Tissue, Graduate School of Dental Medicine, and Faculty of Dental Medicine, Hokkaido University, Kita 13 Nishi 7 Kita-ku, Sapporo, 060-8586, Japan. E-mail: amizuka@den.hokudai.ac.jp.

Abstract

To elucidate the effect of evocalcet, a new oral calcimimetic to bone of secondary hyperparathyroidism (SHPT) with chronic kidney disease (CKD), the rats were 5/6 nephrectomized and fed on a high-phosphate diet. The treated rats were then divided into vehicle groups and evocalcet administered groups. The rats in the vehicle groups exhibited increased levels of serum PTH and inorganic phosphate (Pi) levels, high bone turnover, and severe cortical porosity, mimicking SHPT (CKD-SHPT rats). The cortical bone of the CKD-SHPT rats showed broad demineralization around the osteocytes, suppression of Phex/small integrin-binding ligand N-linked glycoprotein-mediated mineralization in the periphery of the osteocytic lacunae, and increased levels of osteocytic cell death, all of which were considered as the first steps of cortical porosity. In contrast, evocalcet ameliorated the increased serum PTH levels, the enlarged osteocytic lacunae, and the cortical porosity of the CKD-SHPT rats. Osteocytes of CKD-SHPT rats strongly expressed PTH receptor and Pit1/Pit2, which sense extracellular Pi, indicating that PTH and Pi affected these osteocytes. Cell death of cultured osteocytes increased in a Pi concentration-dependent manner, and PTH administration rapidly elevated Pit1 expression and enhanced osteocytic death, indicating the possibility that the highly concentrated serum PTH and Pi cause severe perilacunar osteolysis and osteocytic cell death. It is likely therefore that evocalcet not only decreases serum PTH but also reduces the exacerbation combined with PTH and Pi to the demineralization of osteocytic lacunae and osteocytic cell death, thereby protecting cortical porosity in CKD-SHPT rats.

Key Words: secondary hyperparathyroidism, evocalcet, cortical porosity, osteocyte, Phex/SIBLING

Secondary hyperparathyroidism (SHPT) is a common complication in patients with chronic kidney disease (CKD) and a pathological condition characterized by parathyroid hyperplasia and excessive secretion of PTH (1–3). Abnormalities in serum PTH, inorganic phosphate (Pi), and calcium (Ca) concentrations in SHPT are major factors in CKD, especially mineral and bone disorders (CKD-MBD), leading to ectopic mineralization or bone fractures, which affects prognosis (4, 5). Osteitis fibrosa and severe cortical porosity are the primary abnormalities observed in the bones of patients with SHPT. Cortical porosity increases bone fragility or the risk of fractures, and multiple fractures not only impair the quality of life but also affects the risk of being bedridden or having a healthy life expectancy (6). Therefore, proper SHPT management will improve bone metabolism and reduce the risk of fractures.

CKD patients with SHPT develop various organ disorders because of an increase in serum PTH and fibroblast growth factor 23 (FGF23) or a decrease in 1α,25-dihydroxyvitamin D3 (1α,25(OH)2D3) levels (7). In addition, elevated serum Pi levels in CKD patients with SHPT may directly affect the bone tissue, because the serum Pi levels are regulated in the bone and cardiovascular system in CKD-MBD (8). In particular, serum Pi carries a risk of inducing fracture even in healthy adults when levels are in the normal to high range (9, 10).

Calcimimetics have been used for SHPT treatment in patients undergoing dialysis (11, 12) because they stimulate the Ca receptor in the parathyroid gland to suppress PTH secretion which affects the bone and kidney mediated by the PTH receptor (PTHR) (13, 14). Several effects of calcimimetics on bones have been reported; the BONAFIDE study compared bone tissues from dialysis patients before and after treatment with cinacalcet hydrochloride (cinacalcet), a former-generation calcimimetic, and demonstrated that the long-term administration of cinacalcet reduces the serum PTH levels and attenuates the increase in markers of bone turnover (15). In addition, a subanalysis of the EVOLVE study involving patients undergoing dialysis with SHPT verified that cinacalcet significantly reduces the fracture risk (16).

Evocalcet was launched in 2018 as a new oral calcimimetic agent in Japan (17, 18). Similar to cinacalcet, evocalcet reduces serum PTH levels by acting allosterically on the Ca receptor and alleviates the side effects on the upper gastrointestinal tract, such as nausea and vomiting (19–21). Thus, evocalcet

Received: 18 October 2022. **Editorial Decision:** 25 January 2023. **Corrected and Typeset:** 20 February 2023

enables good mineral management in dialysis patients with SHPT and may contribute to the normalization of bone turnover and reduction of the fracture risk in these patients. However, the effects of evocalcet on SHPT-induced bone abnormalities, such as severe cortical porosity, remain unknown. Therefore, the molecular and cellular mechanisms of the initiation of SHPT-driven cortical porosity, which increases bone fragility or the risk of fractures, should be determined. Clinically, studies should also clarify whether evocalcet can improve the SHPT-induced cortical porosity.

In this study, therefore, we investigated the molecular and cellular mechanisms underlying the bone abnormalities associated with cortical porosity and the effects of evocalcet on cortical porosity using SHPT model rats subjected to 5/6 nephrectomy and fed a high-Pi diet (CKD-SHPT rats).

Materials and Methods

Test Articles

Evocalcet was synthesized by Mitsubishi Tanabe Pharma Corporation and prepared for oral administration by suspending in a 0.5% methylcellulose solution. For continuous administration through subcutaneous (SC) implantation, after being suspended in a lipid emulsion (composition: ethanol, Egg-PC, soybean oil, oleic acid, saline, PEG-DSPE), evocalcet was infused into a microinfusion pump (iPRECIO® SMP-200; Primetech Corporation, Tokyo, Japan).

Animal and Tissue Preparation

Six-week-old male Sprague-Dawley rats (Charles River Laboratories Japan Co., Ltd., Kanagawa, Japan) were used in the experiment after 1 week of preliminary breeding. The rats were kept at 20°C to 26°C and 30% to 70% humidity under a 12-hour light-dark cycle with ad libitum access to tap water. All animal studies were conducted in strict accordance with the Standards for Proper Conduct of Animal Experiments at Kyowa Kirin Co., Ltd. The protocol was approved by the Institutional Animal Care and Use Committee of Kyowa Kirin Co., Ltd. (approval number APS 17J0266 and 18J0242).

After 1 week of acclimatization, approximately two-thirds of the left kidney of 7-week-old rats were resected under anesthesia with pentobarbital (50 mg/kg BW, intraperitoneally) and buprenorfin (0.04 mg/kg BW, subcutaneously). They were resected again 1 week later in a similar manner by fully removing the right kidney under anesthesia to create a 5/6 nephrectomy group. The sham group received 2 bilateral surgeries with the same timing as that of the 5/6 nephrectomy group; the 7-week-old rats received sham operations on the left side after 1 week of acclimatization and a sham operation on the right side after another week (at 8 weeks old) while under anesthesia.

For postoperative management, all operated rats were given buprenorphine (0.04 mg/kg BW, subcutaneously) the day after surgery. They had unrestricted access to standard rodent diet (FR-2; Funabashi Farm Co., Ltd., Chiba, Japan) for another week. After nephrectomy, 9-week-old rats were subjected to a high-phosphate diet containing 0.6% Ca and 1.2% phosphate (Oriental Yeast Co., Ltd., Tokyo, Japan) for 8 weeks to induce SHPT (Fig. 1A).

Since an adriamycin-induced renal failure model demonstrated that the decreased bone mineral density was significantly improved by receiving another calcimimetic daily oral administration, but not continuous administration (22), this study employed 3 patterns of once a day (QD), once every 2 days (Q2D), and continuous administration. The 5/6 nephrectomized rats were divided into the following groups: oral vehicle administration (vehicle PO group), oral evocalcet (0.3 mg/kg BW) with once-daily administration (Evo QD group), and oral evocalcet with administration once every 2 days (Evo Q2D group). The following groups were also prepared: vehicle administration (vehicle SC group, where a microinfusion pump with a pump flow rate of 10 µL/h was subcutaneously embedded) and continuous evocalcet (1 mg/mL) administration (Evo SC group; n = 10 per group). Additional rats were prepared in each of these groups for gene expression analysis at the midpoint of the experimental periods (3 weeks after drug administration, n = 5 per group).

For the bone histomorphometrical analysis, calcein (8 mg/kg BW) and tetracycline hydrochloride (30 mg/kg BW) were injected on days 10 and 3, respectively, before the rats were sacrificed. The blood samples in all groups were collected 1 hour after the administration of vehicle or evocalcet on day 3 to verify the early pharmacological effects of evocalcet. The serum concentrations of intact PTH, Ca, Pi, FGF23, 25-hydroxyvitamin D (25(OH)D), type 1 amino-terminal propeptide (PINP), and type I collagen cross-linked C-telopeptide (CTX) were measured as described later.

After 6 weeks of drug administration, ie, at the endpoint of the experiments, blood samples were collected from the abdominal aorta or left ventricle of all rats after they had been anesthetized with isoflurane inhalation. The left femora were then immediately extracted, frozen in liquid nitrogen for the gene expression analysis, and stored at −80°C until RNA extraction. The left tibiae were frozen in liquid nitrogen for the bone strength test, and the right femora were fixed with 4% paraformaldehyde diluted in 0.1 M phosphate buffer (pH 7.4) for 24 hours. Afterward, microcomputed tomography (CT) was performed. For the histological analysis, the right femora were decalcified with 10% ethylenediaminetetraacetic acid disodium salt solution and embedded in paraffin. The right tibiae were immersed in 70% ethanol solution for the bone histomorphometry analysis. A part of the femora was immersed in 1/2 Karnovsky and post-fixed with osmium tetroxide in 0.067 M cacodylate buffer (pH 7.4). After being dehydrated with acetone, undecalcified femora were embedded in epoxy resin (Epon 812; Taab Co., Ltd., Berks, UK) for the microstructural analysis.

Biochemical Analyses of Serum Markers

Serum markers were measured using the following assay reagents: serum intact PTH, rat intact PTH ELISA kit (cat. no. 60-2500, Immutopics, Inc., San Clemente, CA, USA, RRID: AB_2827505); serum Ca, Calcium E-Test Wako (FUJIFILM Wako Pure Chemical Corporation, Osaka, Japan); serum Pi, Phospha C-Test Wako (FUJIFILM Wako Pure Chemical Corporation); serum FGF23, FGF23 ELISA kit (cat. no. CY-4000, KAINOS Laboratories, Inc., Tokyo, Japan, RRID: AB_2782966); serum 25(OH)D direct day ELISA Kit (cat. no. KR2108, Immundiagnostik AG, Bensheim, Germany, RRID: AB_2927705); PINP, rat/mouse PINP EIA (cat. no. AC-33F1, Immunodiagnostic Systems Ltd, Boldon, UK, RRID: AB_2801263); and CTX, Rat Laps EIA kit (cat.

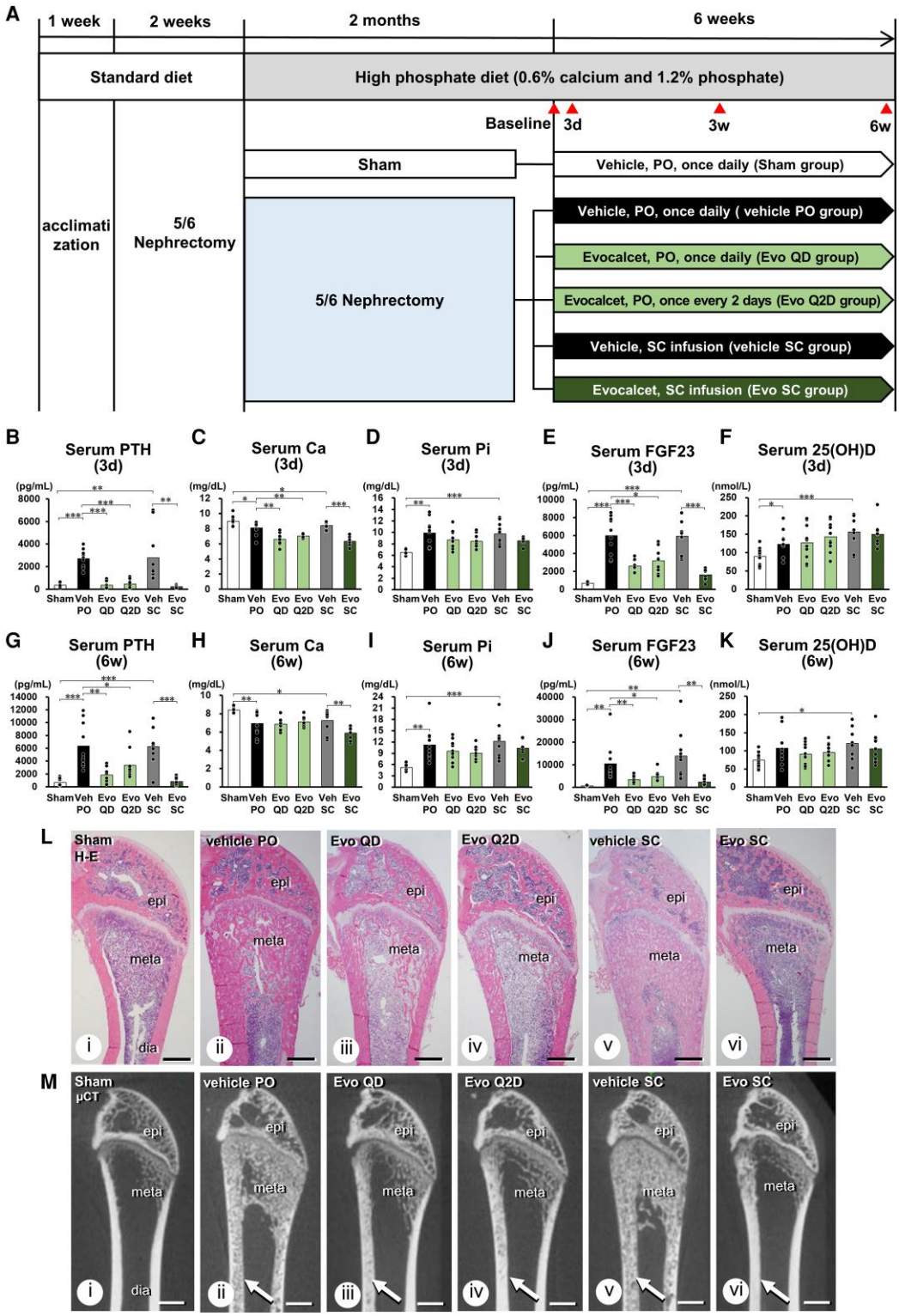

Figure 1. Serum markers and bone tissue of CKD-SHPT rats with secondary hyperparathyroidism. (A) Experimental design. Vehicle PO group, oral vehicle administration; Evo QD group, oral evocalcet (0.3 mg/kg BW) administration once daily; Evo Q2D group, oral evocalcet administration once every 2 days; vehicle SC group, continuous vehicle administration; Evo SC group, continuous evocalcet (1 mg/mL) administration. (B-F) Levels of indicated serum markers 3 days after evocalcet administration (n = 10 per group). (G-K) Levels of indicated serum markers 6 weeks after evocalcet administration (n = 10 per group). Data are shown as the mean ± SE; differences with $P < 0.05$ were considered significant (see Methods). ***, $P < 0.001$; **, $P < 0.01$; *, $P < 0.05$. (L) Images of (H-E) staining of the rat femora after 6 weeks of evocalcet administration. Many cancellous bones were found in the metaphysis, and cortical porosity was observed in the vehicle groups (ii, v). In the Evo groups (iii, iv, vi), the volume of cancellous bones was similar to that in the sham group (i), and only a few pores were detected in the cortical bone. (M) Micro-computed tomography image of the femora after 6 weeks of evocalcet administration. Cancellous bones with a developed meshwork structure are observed in the metaphysis of the vehicle groups (ii, v). Many transparent patched areas can be seen throughout the cortical bone (arrows, ii, v). In the Evo groups (iii, iv, vi), the number of cancellous bones is the same or slightly more than that in the sham group (i), and the cortical bone show a radio-opaque profile (arrows, iii, iv, vi). Scale bars, 1 mm.

Abbreviations: dia, diaphysis; epi, epiphysis; meta, metaphysis.

no. AC-06F1, Immunodiagnostic Systems Ltd., RRID: AB_2801265).

Bone Histomorphometry

The right tibiae were cut 2 cm distal from the proximal articular surface, where the proximal part was taken as a cancellous bone sample, while the central part of the tibiae was collected as a cortical bone sample (MC-130D/Maruto Instrument Co., Ltd., Tokyo, Japan). These samples were immersed in Villanueva Bone stain solution and then embedded in methyl methacrylate resin. Sagittal sections were prepared from cancellous bone samples, while horizontal sections were prepared from cortical bone samples for bone morphological measurement. The assumed boxed areas of the sagittal section in the cancellous bone (height, from 1.40 mm to 1.29 mm away from the bottom of the growth plate; width, 5.70 mm) were used for the histomorphometrical analysis of bone volume/tissue volume (BV/TV, %), trabecular number (Tb.N, N/mm), trabecular thickness (Tb.Th, μm), osteoblast surface (Ob.S, μm), bone formation rate/tissue volume (BFR/TV, %/y), mineral apposition rate (MAR, μm/day), osteoid volume/tissue volume (OV/TV, %), and osteoclast number (Oc.N, N) (23). Cortical porosity (Ct.P, %) was measured throughout the horizontal sections of the cortical bone. Ct.P was defined as a hole inside the cortical bone without continuity in bone marrow areas.

Bone Strength Measurement

The left tibiae were subjected to a 3-point bending test using a bone-strength measuring device (MZ-500D; Maruto Instrument Co., Ltd.). According to previous reports (24, 25), the length of the tibiae from the proximal articular surface to the distal termini was measured to determine the center of the tibial mid-shaft. The crosshead of the loading was positioned at the central point of the mid-shaft. Each tibia was placed with the medial part facing down on 2 supporting bars with a distance of 16 mm and then weighted from the external face at a load rate of 2 mm/min. The ultimate load (N), displacement at yield (mm), stiffness (N/mm), and energy (N·mm) were obtained as the output based on the measured data.

Micro-CT Analysis

Micro-CT images of the sagittal section in the right femora from the end of the distal epiphysis to 1.6 cm distally were obtained with micro-CT (CosmoScan Fx; Rigaku Corporation, Tokyo, Japan) at a tube voltage of 90 kV and tube current of 88 μA (FOV 25 mm).

Histochemical Staining

After being embedded in paraffin, the deparaffinized sections were washed with PBS and immersed in 0.3% hydrogen peroxide solution in PBS for 30 minutes. The blocking treatment of the nonspecific reaction was performed using 1% BSA (Seologicals Proteins Inc., Kankakee, IL, USA) in PBS. The primary and secondary antibodies used are shown in Table 1, and immunostaining was performed as described by Hasegawa et al (28, 29). After incubation with the secondary antibody, immunoreaction was visualized using 3,3′-diaminobenzidine tetrahydrochloride (Dojindo Laboratories, Kumamoto, Japan). The epoxy resin-embedded undecalcified sections were reacted with an aqueous solution of 1% silver nitrate for von Kossa staining to visualize the mineralized bone matrix.

Measurement of TUNEL-positive Osteocytes, Osteocytic Lacuna Perimeter, Osteocytic Lacuna Area, Percentage of Empty Lacunae, and Percentage of Calcein/Tetracycline Positive Osteocytic Lacunae

Deparaffinized sections were washed with PBS and then reacted using a Trevigen TACS 2TdT-DAB In Situ Apoptosis Detection Kit (R&D Systems, Inc., Minneapolis, MN, USA) to detect osteocytic apoptosis. The percentage of terminal deoxynucleotidyl transferase-mediated dUTP nick-end labeling (TUNEL)-positive osteocytes was obtained by dividing the number of TUNEL-positive osteocytes by the total number of osteocytes. Using the Villanueva-stained section, osteocytic lacuna perimeter (Ocy. Lc. Pm, μm), osteocytic lacuna area (Ocy. Lc. Ar, μm^2), percentage of empty lacunae, and percentage of calcein/tetracycline-positive osteocytic lacunae were measured using the Image-Pro Plus 6.2 software program (Media Cybernetics, Inc., Bethesda, MD, USA). All measurements were performed in the cortical bone region from 1.5 mm to 2.0 mm proximal to the distal metaphyseal growth plate.

The Quantitative Analysis of Gene Expression Through RT-qPCR

The cortical bone of the left femora (n = 5 per group) at the midpoint (3 weeks) of the experimental period and the whole left femora (n = 10 per group) at the endpoint (6 weeks) of the experimental period were used for real-time PCR. Bone samples were frozen in liquid nitrogen and ground with a multi-bead shocker (MB3200S; Yasui Kikai Co., Osaka, Japan). The powdered samples were homogenized by adding 10 mL/g of TRIzol reagent (Life Technologies Co., Carlsbad, CA, USA). Then 2 mL of chloroform was added to 10 mL of TRIzol solution; the mixture was stirred for 15 seconds and incubated at room temperature for 5 minutes. The mixture was centrifuged at 15 000 rpm at 4 °C for 15 minutes to extract the total RNA from the aqueous layer using the PureLink RNA Mini Kit (Life Technologies Co.). First-strand cDNA was synthesized from the obtained total RNA with the SuperScript VlLO cDNA Synthesis Kit (Life Technologies Co.). The expression levels of various genes relative to those of *Gapdh* were comparatively quantified via the ΔΔCt method in a quantitative PCR System (StepOne; Thermo Fisher Scientific Inc., Waltham, MA, USA) for the expression of *Alp*, *Trap*, *Rankl*, *Rank*, *Opg*, *Fgf23*, *Fgfr1*, *Pth1r*, *Dmp1*, *Mepe*, *Cathepsin b*, *Phex*, *Pit1*, and *Pit2*. The TaqMan probes (Applied Biosystems, Waltham, MA, USA) used for the analysis are shown in Supplemental Table 1 (30).

RNA Sequencing Analysis

The total RNA obtained from the left femora of the sham, vehicle PO, and Evo QD groups at the endpoint was employed for the RNA sequencing analysis (n = 3 per group). The base sequences of the library-adjusted sample were obtained (acquired read length: 150 bp × 2 paired ends) using the next-generation sequencer NovaSeq 6000 (Illumina, Inc., San Diego, CA, USA) and the library adjustment reagent NEBNext Ultra II Directional RNA Library Prep Kit (E7760; New England

Table 1. List of primary/secondary antibodies used in this study

Primary antibody	Cat. no.	Company	Dilution	RRID
Rabbit polyclonal antisera against TNALPase		Provided by Dr. Oda[26]	1: 300	AB_2722759
Rat monoclonal anti-FGF23	MAB26291	R&D systems, Inc., Minneapolis, MN	1: 100	AB_2104623
Mouse anti-human cathepsin K	F-95	Daiichi Fine Chemical Co., Ltd., Takaoka, Japan	1: 200	AB_2927739
Rabbit polyclonal anti-ATP6V0D2/V-ATPase D2	bs-12548R	Bioss Inc., Boston, MA	1: 100	AB_2927740
Rabbit antibody against DMP1	M176	Takara Bio Inc., Otsu, Japan	1: 200	AB_2722758
Rabbit polyclonal anti-MEPE	PAB232Ra01	Cloud-Clone Corp., Katy, TX	1: 100	AB_2927741
Rabbit polyclonal anti-Phex	CSB-PA017896LA01HU	Cusabio Technology LLC, Houston, TX	1: 100	AB_2927742
Rabbit polyclonal anti-cathepsin B	12216-1	Proteintech Group, Inc., Rosemont, IL	1: 100	AB_2086929
Human anti-phosphorylated ASARM peptide		Bio-Rad AbD Serotec GmbH. Inc., Puchheim, Germany, GeneFrontier Corp., Kashiwa, Japan, provided by Dr. Yoshiko[27]	1:100	AB_2927781
Rabbit antibody against PTH/PTHrP receptor	G220	Assay Biotechnology Company, Inc., Sunnyvale, CA	1: 50	AB_10688207
Mouse monoclonal anti-FGFR1	ab824	Abcam plc., Cambridge, UK	1: 50	AB_306385
Rabbit polyclonal anti-SLC20A1 (Pit1)	GTX105062	GeneTex., Inc., Irvine, CA	1: 100	AB_1951921
Rabbit polyclonal anti-SLC20A2 (Pit2)	12820-1-AP	Proteintec Group., Inc., Rosemont, IL	1: 50	AB_2191004

Secondary antibody	Cat. no.	Company	Dilution	RRID
HRP-conjugated anti-rabbit IgG	P0399	DakoCytomation, Glostrup, Denmark	1: 100	AB_2617141
HRP-conjugated anti-rat IgG	A18921	Zymed Laboratories Inc., South San Francisco, CA	1: 100	AB_2535696
HRP-conjugated anti-mouse IgG	61-6520	Chemicon International Inc., Temecula, CA	1: 100	AB_138451
HRP-conjugated anti-human IgG-(Fab')2	ab98605	Abcam plc., Cambridge, Cambridgeshire, UK	1: 100	AB_10674601
Alexa488-conjugated anti-rabbit IgG	ab150077	Abcam plc., Cambridge, Cambridgeshire, UK	1: 100	AB_2630356

Abbreviations: ASARM, acidic serine aspartate-rich MEPE-associated motif; DMP1, dentin matrix protein 1; FGF23, fibroblast growth factor 23; FGFR, fibroblast growth factor receptor; HRP, horseradish peroxidase; IgG, immunoglobulin G; MEPE, matrix extracellular phosphoglycoprotein.

Biolabs Japan Inc., Tokyo, Japan). Subsequently, the sequence reads were trimmed using Trimmomatic ver. 0.38, and the sequence reads were mapped to the rat reference genome (rn6) using HISAT2 ver. 2.1.0. The number of raw reads mapped to known exon regions, FRKM, and TPM were calculated using featureCounts ver. 1.6.3 to quantify the gene expression. The differentially expressed genes in the sham, vehicle PO, and Evo QD groups were extracted using DeSeq2 (ver. 1.24.0) to create a heatmap.

In Vitro Experiments on the Gene Expression and Death of MLO-Y4 Cells

Mouse osteocyte cell line MLO-Y4 cells (31) (2×10^5 cells; Kerafast, Inc., Boston, MA, USA) were seeded in a T25 flask containing an α-MEM (FUJIFILM Wako Pure Chemical Co.) containing 2.5% fetal bovine serum (Hyclone # SH30396; Cytive, Tokyo, Japan) and 2.5% calf serum (Hyclone # SH30072, Cytive) and then incubated in a 5% CO_2 incubator for 24 hours. The dose of human PTH[1-34] (hPTH[1-34]; Merck KGaA, Darmstadt, Germany), Pi (Na_2HPO_4/NaH_2PO_4, pH 7.4), and recombinant human FGF23 (hFGF23; R&D Systems) administered to MLO-Y4 cells were adjusted to be similar to the serum concentrations of the molecules derived from CKD rats in order to examine the effects of PTH, Pi, and FGF23 on the gene expression of osteocytes in vitro. In particular, MLO-Y4 cells were replaced with a culture medium supplemented with one of the following reagents: 0.1, 1.0, or 10 mM hPTH[1-34]; 1.0, 5.0, or 10.0 mM of Pi; 5, 10, or 50 ng/mL hFGF23; and Pi + hPTH[1-34] mixtures (0.1 mM hPTH[1-34] + 1.0 mM Pi, 1.0 mM hPTH[1-34] + 5.0 mM Pi, or 10 mM hPTH[1-34] + 10 mM Pi). MLO-Y4 cells were treated with these culture media for 3, 6, 12, or 24 hours (n = 3). After the treatments, the cells were collected, total RNA was extracted, the first-strand cDNA was synthesized, and the expression levels of *Pit1*, *Pit2*, *Alp*, *Enpp1*, *Rankl*, *Opg*, *Fgfr1*, *Pthr*, *Dmp1*, *Phex*, *Acp1*, and *Galnt3* were analyzed by quantitative PCR and normalized to *Gapdh* expression via the ΔΔCt method. The TaqMan probes used for the analysis are as shown in Supplemental Table 1 (30). MLO-Y4 cells were cultured in the same culture medium containing hPTH[1-34], Pi, hFGF23, and hPTH[1-34] and Pi mixture as described previously for 1, 2, and 3 days (n = 4) to assess the death of MLO-Y4 cells under highly concentrated hPTH[1-34], Pi, or hFGF23. The cells in the supernatants of the culture media were then collected and counted after trypan blue staining. To achieve the immunolocalization of Pit1 and Pit2, which are phosphate sodium co-transporter type III, in the cultured MLO-Y4 cells after Pi treatment, MLO-Y4 cells were treated with 0.25% fetal bovine serum + 0.25% calf serum-containing α-MEM for 10 minutes and then cultured in α-MEM with 10 mM Pi for 6 or 12 hours prior to immunostaining. The primary and secondary antibodies for Pit1 and Pit2 immunostaining are shown in Table 1.

Statistical Analyses

Data are shown as the mean ± SE. Animal experiments were statistically analyzed using the SAS software (release 9.4; SAS Institute, Inc., Cary, NC, USA). For comparisons between the sham and vehicle PO groups or the vehicle SC group, student's *t*-test was conducted if no difference in variance was observed after an F-test, while an Aspin-Welch test was performed if a difference in variance was found. For comparisons between the vehicle PO and Evo QD groups or the Evo Q2D group, a Kruskal-Wallis test was conducted if the variance differed after a Bartlett test. A Steel test was further conducted if a significant difference was found. If no difference was found following the Bartlett test, a one-way ANOVA was conducted, while Dunnett's test was further performed if differences were significant. For comparisons between the vehicle SC group and the Evo SC group, after an F-test, student's *t*-test was conducted if the variance had no difference, while an Aspin-Welch test was performed if the variance differed. In each case, a *P* value of less than 0.05 was considered to indicate a significant difference. The BellCurve for Excel software (Social Survey Research Information Co., Ltd., Tokyo, Japan) was used to statistically analyze in vitro experiments involving MLO-Y4 cells. The significance of differences was determined through a one-way ANOVA followed by Dunnett's test for multiple comparisons (PTH, Pi, PTH + Pi, and FGF23-added medium groups).

Results

Evocalcet Reduces the Serum PTH and FGF23 Levels in 5/6 Nephrectomized Rats With High-Pi Load (CKD-SHPT Rats)

Serum markers such as PTH, Ca, Pi, FGF23, and 25(OH)D were measured in samples collected from sham rats, nephrectomized rats, and evocalcet-treated nephrectomized rats 3 days after the evocalcet administration to verify the early effects of evocalcet in a state of SHPT induced by 5/6 nephrectomy with a high Pi diet (Fig. 1B-F). In nephrectomized rats in the vehicle PO and vehicle SC groups, the serum PTH, Pi, FGF23, and 25(OH)D levels markedly increased compared with those in the sham group. The serum PTH, Ca, and FGF23 levels in the evocalcet-treated nephrectomized rats (Evo QD and Evo Q2D groups) significantly reduced compared with those in the vehicle PO group, but the Pi and 25(OH)D levels did not decrease. The serum markers were also examined at the endpoint (6 weeks) of the experimental period (Fig. 1G-K). In the vehicle groups, the serum PTH, Pi, and FGF23 levels significantly increased; conversely, the serum Ca levels significantly decreased compared with those in the sham groups. The serum PTH and FGF23 levels in all the evocalcet-treated groups (Evo QD, Evo Q2D, and Evo SC groups) were significantly lower than those in the vehicle groups. The serum Pi levels decreased in all evocalcet-treated groups, although the values did not significantly differ from those in the vehicle groups.

Evocalcet Ameliorates Cancellous Bone Abnormalities Caused by SHPT

Hematoxylin-eosin staining (Fig. 1L) and micro-CT (Fig. 1M) showed a large amount of cancellous bone and severe cortical porosity in the femora of the vehicle groups. In the Evo groups, the amount of cancellous bone was markedly reduced, and cortical porosity was recovered to levels similar to those in the sham group (Fig. 1L and 1M). Consistently, bone histomorphometrical parameters, such as BV/TV, Tb/N, and Tb/Th of cancellous bone, were higher in the vehicle groups than in the sham group but decreased in the Evo Q2D and Evo SC groups to the same extent as in the sham group (Fig. 2A–C). The indices of BFR/TV, MAR, Ob.S, Oc. N, and OV/TV were significantly higher in the vehicle groups than in the sham group. In the Evo QD/Q2D groups, these values decreased but did not significantly differ from those in the vehicle group (Fig. 2D-H). PINP and CTX levels were significantly increased in the vehicle groups compared with those in the sham group but were decreased in the Evo QD and Q2D groups and significantly decreased in the Evo SC group (Fig. 2I and 2J).

Six weeks after evocalcet administration, the femora in the vehicle groups, compared with those in the sham groups, showed a large number of alkaline phosphatase (ALP)-positive osteoblasts and preosteoblasts forming a thick cell layer (Fig. 2Q), a thick osteoid beneath the mature osteoblasts (Supplemental Fig. 1A) (30), and tetracycline and calcein labeling intricately deposited on the cancellous bone (Supplemental Fig. 1B) (30). In the vehicle group, many TRAP-positive osteoclasts were observed in the thick ALP-positive cell layer (Fig. 2R), and the immunoreactivity of FGF23 was seen not only in osteocytes but also in the thick osteoblastic cell layer (Fig. 2S). In the Evo groups, the ALP-positive cell layer, the number of TRAP-positive osteoclasts, and the FGF23-positive reaction were attenuated. Consistently, the mRNA expression levels of *Alp*, *Rank*, and *Opg* in the Evo QD and Q2D groups were lower than those in the vehicle groups, although no significant differences were observed. The expression levels of *Trap* and *Fgf23* in the Evo QD and Q2D groups and *Rankl* in the Evo QD group significantly decreased compared with those in the vehicle groups (Fig. 2K-P).

Therefore, CKD-SHPT rats were characterized by a high bone turnover with stimulated bone formation and bone resorption in the cancellous bone; however, evocalcet suppressed bone resorption and bone formation.

Evocalcet Suppresses SHPT-induced Cortical Porosity

The cortical bones in the vehicle groups mimicking SHPT showed a severely porous structure, ie, cortical porosity, and many cathepsin K-positive osteoclasts and ALP-positive osteoblasts had invaded therein (Fig. 3A-C). Many complicated calcein/tetracycline labeled areas were observed in the pore region of the cortical bone (Fig. 3D), strongly suggesting a high bone turnover with active bone remodeling. In the Evo groups, however, cortical porosity was suppressed, showing less invasion of osteoclasts or osteoblasts (Fig. 3A-C) and reduced calcein/tetracycline labeling (Fig. 3D). The rate of Ct.P significantly increased in the vehicle PO group compared with the sham group but significantly decreased in the Evo QD and Q2D groups compared with the vehicle PO group (Fig. 3E). Bone strength measurements revealed significantly diminished indices of ultimate load, displacement at yield, and energy in the vehicle PO groups compared with the sham groups (Fig. 3F-I). The ultimate load and stiffness in the Evo SC group and the energy in the Evo QD and Evo SC groups were significantly higher than those in the corresponding vehicle groups (Fig. 3F, 3H, 3I).

Thus, CKD-SHPT rats exhibited severe cortical porosity and decreased bone strength; conversely, evocalcet recovered the cortical porosity and bone strength.

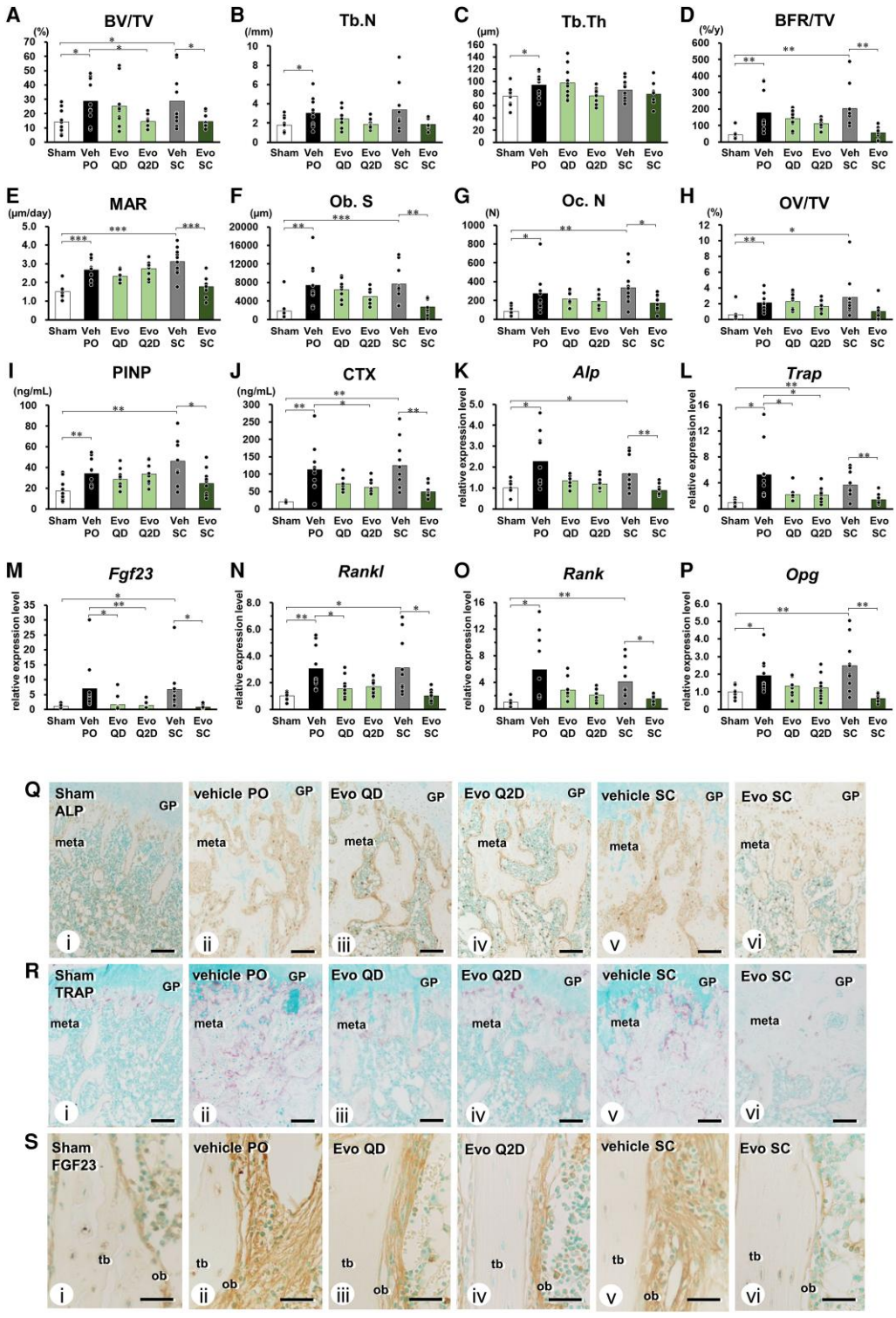

Figure 2. Histomorphometry of the cancellous bone of CKD-SHPT rats with secondary hyperparathyroidism. (A-H) Histomorphometrical analyses of the cancellous bone in the metaphysis after 6 weeks of evocalcet administration (n = 10 per group). (A) Bone volume (BV/TV). (B) Trabecular number (Tb.N). (C) Trabecular thickness (Tb.Th). (D) Bone formation rate (BFR/TV). (E) Mineral apposition rate (MAR). (F) Osteoblast surface (Ob.S). (G) Osteoclast number (Oc.N). (H) Osteoid volume (OV/TV). (I-J) Indicated serum parameters of bone formation and resorption 6 weeks after evocalcet administration (n = 10 per group). (K-P) Expression of indicated osteoblast/osteoclast-related genes in the femora after 6 weeks of evocalcet administration (n = 10 per group). The data in are shown as the mean ± SE. Differences with $P < 0.05$ were considered significant (see Methods). ***, $P < 0.001$; **, $P < 0.01$; *, $P < 0.05$. (Q-S) Histological images of (Q) ALP immunostaining (brown; scale bars, 200 μm), (R) TRAP staining (red; scale bars, 200 μm), and (S) FGF23 immunostaining (brown, scale bars, 20 μm). In the vehicle groups (ii, v), numerous ALP-positive osteoblasts (brown) and TRAP-positive osteoclasts (red) were observed in the metaphyseal trabeculae. In the Evo groups (iii, iv, vi), reduced thickness of ALP-positive osteoblastic cells (brown) and lower number of TRAP-positive osteoclasts (red) were seen; the number of ALP-positive osteoblasts and TRAP-reactive osteoclasts was equivalent to or slightly higher than that in the sham group (i).

Abbreviations: ALP, alkaline phosphatase; FGF23, fibroblast growth factor 23; GP, growth plate; meta, metaphysis; ob, osteoblast; tb, trabecular bone.

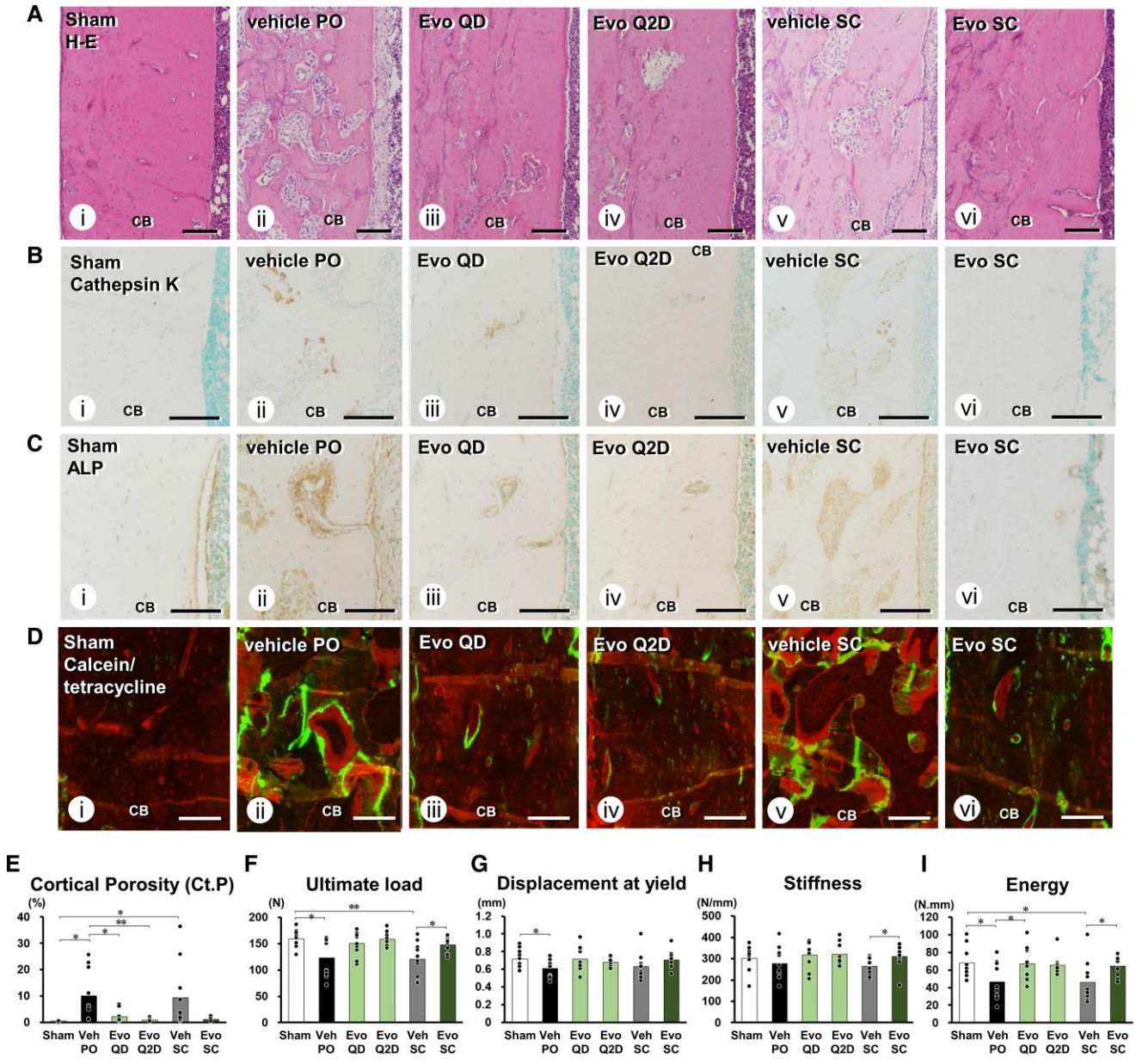

Figure 3. Histology and mechanical strength of the cortical bone of CKD-SHPT rats. (A–C) Histology of the femoral cortical bone after 6 weeks of evocalcet administration (scale bars, 100 μm). (A) Cortical bones with many pores in the vehicle group (ii, v), cortical bones featuring only a few porous structures in the Evo group (iii, iv, vi) similar to those in the sham group (i). (B) Immunolocalization of cathepsin K (brown). (C) Distribution of ALP (brown). Many cathepsin K-positive osteoclasts and ALP-positive osteoblasts were observed inside the cortical bone in the vehicle group (ii, v) but not in the Evo group (iii, iv, vi). (D) Calcein/tetracycline labeling in the undecalcified cortical bone after 6 weeks of evocalcet administration (scale bars, 40 μm). Numerous regions positive for calcein (green) or tetracycline (yellow green) labeling were found inside the cortical bone in the vehicle group (ii, v). In the Evo group (iii, iv, vi), only a few areas with calcein/tetracycline were observed. (E) The rate of cortical porosity (Ct.P) in the vehicle group was higher than that in the sham group. (F-I) Measures of bone strength after 6 weeks of evocalcet administration (n = 10 per group). (F) Ultimate load. (G) Displacement at yield. (H) Stiffness. (I) Energy. Ultimate load and energy levels in the vehicle PO and vehicle SC groups were lower than those in the sham groups. In the Evo groups, the ultimate load and energy significantly increased compared with those in the corresponding vehicle groups. Data are shown as the mean ± SE; differences with $P < 0.05$ were considered significant (see Methods). ***, $P < 0.001$; **, $P < 0.01$; *, $P < 0.05$.

Abbreviations: ALP, alkaline phosphatase; CB, cortical bone.

Evocalcet Inhibited SHPT-induced Broad Demineralization Around Osteocytes in Cortical Bone

Von Kossa staining indicative of matrix mineralization revealed osteocytes localized in smooth oval osteocytic lacunae in well mineralized matrix of the sham group (Fig. 4A). However, in the vehicle groups, many osteocytes were seen in the enlarged, irregularly shaped lacunae, suggesting the osteocytic osteolysis that bone minerals around the osteocytes were dissolved (Supplemental Fig. 2) (30). In the Evo groups, the enlarged osteocytic lacunae were reduced, while the walls of osteocytic lacunae still exhibited a rough surface. Although the osteocytes of the vehicle groups showed reactivities to acid phosphatase and H^+-ATPase/d2-subunit, these reactivities were not found in the osteocytes of the sham and Evo groups (Fig. 4B and 4C). The indices of the Ocy. Lc. Pm and Ocy. Lc.

Ar as well as the percentage of acid phosphatase-positive osteocytes significantly increased in the vehicle group compared with the sham group, but the indices in the Evo groups decreased to levels similar to those observed in the sham group (Fig. 4D-F). The RNA sequencing analysis of the sham, vehicle PO, and Evo QD groups indicated that the expression levels of the genes related to vacuolar-type ATPase proton pumps, carbonic anhydrases, acid phosphatases, cathepsins, and matrix metalloproteinases increased in the vehicle PO group compared with the sham groups (Fig. 4G). Conversely, their expression in the Evo QD group decreased.

Phosphorylated ASARM Peptide Indicative of Inhibited Mineralization was Detected in the Vicinity of Osteocytes in a SHPT State

The calcein/tetracycline labeling, ie, Ca deposition, was found in a few osteocytic lacunae in the sham group; however, no labeling was observed in the enlarged lacunae of the vehicle groups (Fig. 5A). Interestingly, in the Evo groups, calcein/tetracycline labeling was detected in many osteocytic lacunae. The percentage of calcein/tetracycline-positive osteocytes in the Evo groups were significantly higher than those in the vehicle groups (Fig. 5G).

Next, we focused on Phex/the small integrin-binding ligand N-linked glycoprotein (SIBLING) family, which may inhibit mineralization in the osteocytic lacunae. Although dentin matrix protein 1 (DMP1) was found in all osteocytic lacunae and canaliculi of all groups (Fig. 5B), matrix extracellular phosphoglycoprotein (MEPE) (Fig. 5C) and Phex (Fig. 5D) were more intense in the osteocytic lacunae of the vehicle group. Cathepsin B, an enzyme that breaks down SIBLING family proteins such as DMP1 and MEPE into acidic serine aspartate-rich MEPE-associated motif (ASARM) peptides (Fig. 5E), as well as phosphorylated ASARM peptide (Fig. 5F), were consistently detected in the osteocytes and at their periphery in the vehicle group. At the midpoint (3 weeks) of the experiments, the mRNA expression levels of *Dmp1*, *Mepe*, *cathepsin B*, and *Phex* were markedly elevated in the vehicle groups compared with those in the sham group; however, their expression levels decreased in the Evo groups (Fig. 5H-K). At the endpoint (6 weeks) of the experiment, levels of mRNA encoding *Dmp1* and *Phex* were significantly increased in the vehicle groups but were reduced in the Evo groups (Fig. 5L-O).

Therefore, the cortical bone of CKD-SHPT rats not only induced broad demineralization of in the vicinity of osteocytes but also inhibited mineralization because of the accumulation of the phosphorylated ASARM peptide.

CKD-SHPT Rats Exhibit Osteocytic Cell Death and Empty Lacunae

TUNEL-positive osteocytes and empty lacunae were often observed in the vehicle groups of CKD-SHPT rats (Fig. 6A and 6B). The percentage of TUNEL-positive osteocytes and empty lacunae significantly increased in the vehicle groups (Fig. 6G and 6H). Therefore, we examined whether highly concentrated PTH, FGF23, and Pi induces osteocytic cell death. In the vehicle groups, expression levels of *Pthr* and *Fgfr1* significantly increased (Fig. 6I and 6J), which is consistent with the intense immunoreactivities of PTHR and FGF receptor (FGFR)1 in the osteocytes (Fig. 6C and 6D). Although the immunoreactivity of Pit1, a sodium/phosphate co-transporter type III, was observed in the osteocytes in all groups, Pit2 immunoreactivity was intensely detected in the osteocytes of the vehicle groups (Fig. 6E and 6F). At the midpoint (3 weeks) of the experimental period, *Pit1* and *Pit2* expression levels increased in the vehicle groups compared with those in sham groups but decreased in the Evo groups (Fig. 6K and 6L). At the endpoint (6 weeks), *Pit2* but not *Pit1* levels were elevated in the vehicle groups and decreased in the Evo groups (Fig. 6M and 6N).

Therefore, highly concentrated PTH, FGF23, and Pi derived from SHPT might affect osteocytes, for instance, to dissolve the surrounding bone minerals and cause osteocytic death.

Interactive Effects of Highly Concentrated PTH and Pi on Osteocytic Cell Death

In order to define whether highly concentrated PTH, FGF23, and Pi would affect osteocytes, MLO-Y4 cells were reacted with the culture medium containing hPTH [1-34], Pi, or hFGF23 for 3, 6, 12, and 24 hours. As a result, 1.0, 5.0, and 10.0 mM Pi increased the mRNA levels of *Acp*, *Alp*, *Enpp1*, *Galnt3*, *Phex*, *Dmp1*, *Rankl*, *Opg*, *Pthr*, and *Fgfr1* (Supplemental Fig. 3) (30); conversely, PTH treatment increased the mRNA levels of *Acp*, *Enpp1*, *Phex*, *Dmp1*, *Rankl*, *Opg*, and *Fgfr1* (Supplemental Fig. 3A, C, E-H, J) (30). Although FGF23 treatment promoted the expression of *Enpp1*, *Galnt3*, *Dmp1*, *Opg*, and *Pthr* (Supplemental Fig. 3C, D, F, H, I) (30), the increased levels of these transcripts were lower than those observed in cells treated with Pi or PTH. Interestingly, Pi treatment upregulated expression levels of *Alp*, *Enpp1*, *Phex*, *Dmp1*, and *Pthr*, which are involved in bone mineralization. PTH also increased *Enpp1*, *Phex*, and *Dmp1* levels. Thus, PTH and Pi rather than FGF23 might regulate the expression of mineralization-related genes in bones.

To clarify whether PTH, FGF23, and Pi affect osteocytic cell death, the number of dead MLO-Y4 cells after incubation with Pi, PTH, FGF23, or the Pi + PTH mixture for 1 to 3 days was determined. The numbers of dead cells were significantly higher in the Pi-treated group. Furthermore, in Pi + PTH-treated group, the number of dead cells was much higher than that in the Pi-treated group (Fig. 7A). However, the number of dead MLO-Y4 cells did not increase upon treatment with FGF23 or PTH alone (Fig. 7B and 7C). When MLO-Y4 cells were treated with 10 mM Pi in culture medium, the immunoreactivities of Pit1 and Pit2 were intense initially at the cell membrane but moved to intracellular regions with increased duration of Pi exposure (Fig. 7D). Furthermore, *Pit1* expression increased rapidly after 3 hours but decreased over time after treatments with PTH alone, Pi alone, or PTH + Pi mixture (Fig. 7E and 7F). FGF23 treatment resulted in *Pit1* expression patterns similar those obtained with PTH/Pi treatment (Fig. 7G). Conversely, Pit2 levels slightly increased upon PTH and Pi treatments but did not change in response to with FGF23 treatment (Fig. 7H-J).

Discussion

Our study using CKD-SHPT rats revealed markedly increased serum levels of PTH and Pi, accelerated bone remodeling, and severe cortical porosity bearing bone fragility in these animals. In contrast, evocalcet administration suppressed PTH secretion, diminished high bone turnover, and rescued severe

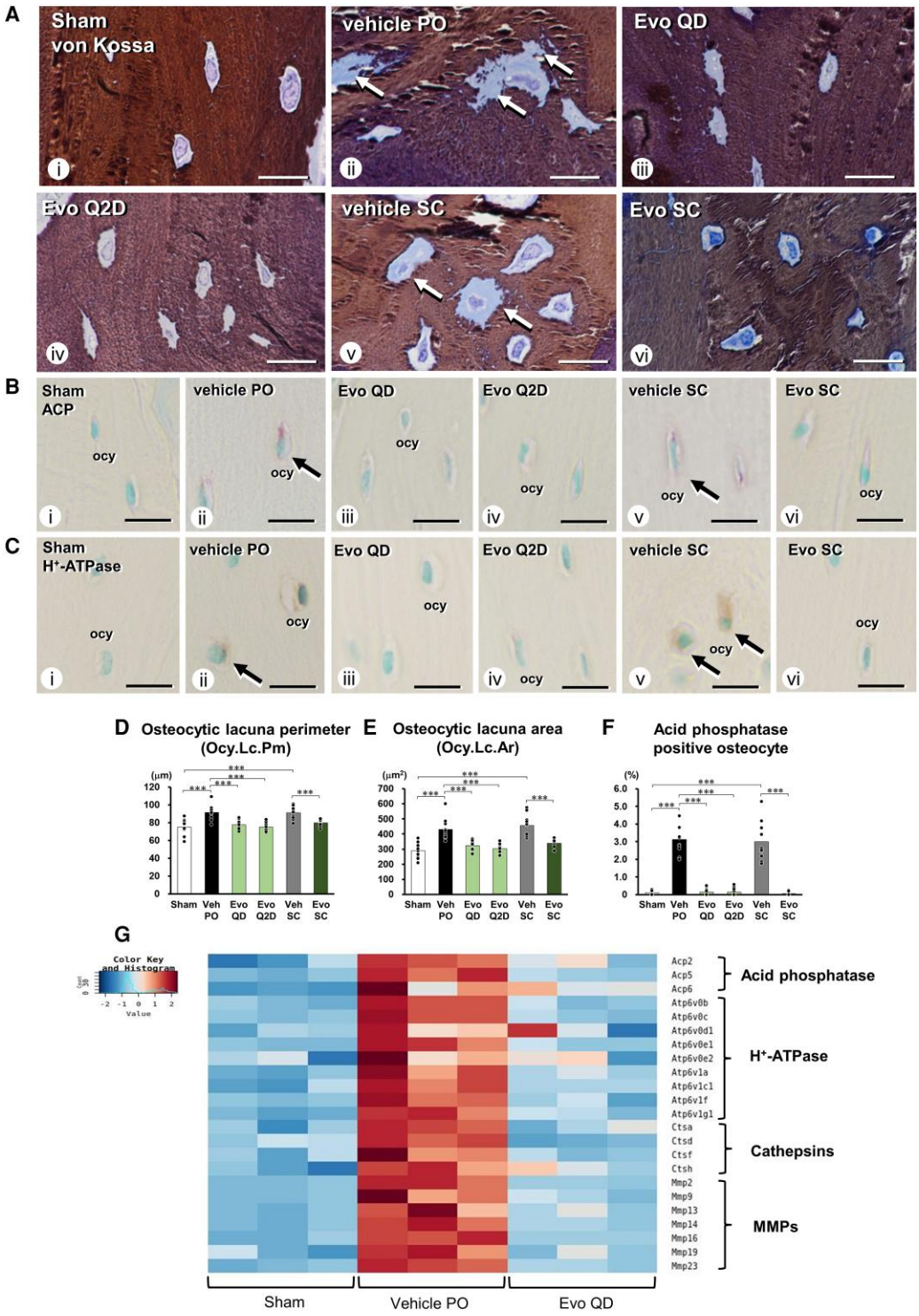

Figure 4. Effect of evocalcet on osteocytic osteolysis in the cortical bone of CKD-SHPT rats. (A-C) Histological images of osteocytic osteolysis in cortical bone after 6 weeks of drug administration. (A) Von Kossa staining visualizing mineralization (dark brown: mineralized bone matrix; light blue: unmineralized matrix containing organic materials such as collagens). Unmineralized matrices (light blue, arrows) are widely found around the osteocytes in the vehicle group (ii, v). In the sham (i) and Evo groups (iii, iv, vi), many osteocytes are surrounded by a mineralized bone matrix (dark brown). Small spaces exist between lacunar walls and osteocytes. Scale bars, 10 μm. (B) Osteocytes in the cortical bone of the vehicle group (ii, v) show acid phosphatase (ACP) staining (arrows, red). (C) Immunohistochemistry of H^+-ATPase (arrows, brown). In the sham (i) and Evo groups (iii, iv, vi), acid phosphatase-positive and H^+-ATPase-positive osteocytes were rarely observed. Scale bars, 10 μm. (D) Osteocytic lacuna perimeter (Ocy.Lc.Pm), (E) osteocytic lacuna area (Ocy.Lc.Ar), and (F) the percentage of acid phosphatase-positive osteocytes after 6 weeks of evocalcet administration (n = 10 per group). Ocy.Lc.Pm, Ocy.Lc.Ar, and percentage of acid phosphatase-positive osteocytes in the vehicle group were higher than those in the sham group. Conversely, the Evo groups showed nearly the same values as the sham groups. Data are shown as the mean ± SE; differences with $P < 0.05$ were considered significant (see Methods). ***, $P < 0.001$; **, $P < 0.01$; *, $P < 0.05$. G. Heatmap of osteolytic osteolysis-related gene expression in the femora of the sham, vehicle PO, and Evo QD group for the RNA sequencing analysis (n = 3). The gene expression of acid phosphatases, various subunits of H^+-ATPase, cathepsins, and MMPs increased in the vehicle PO group (red) but decreased in the Evo QD group (light blue).

Abbreviations: MMPs, matrix metalloproteinases; ocy, osteocyte.

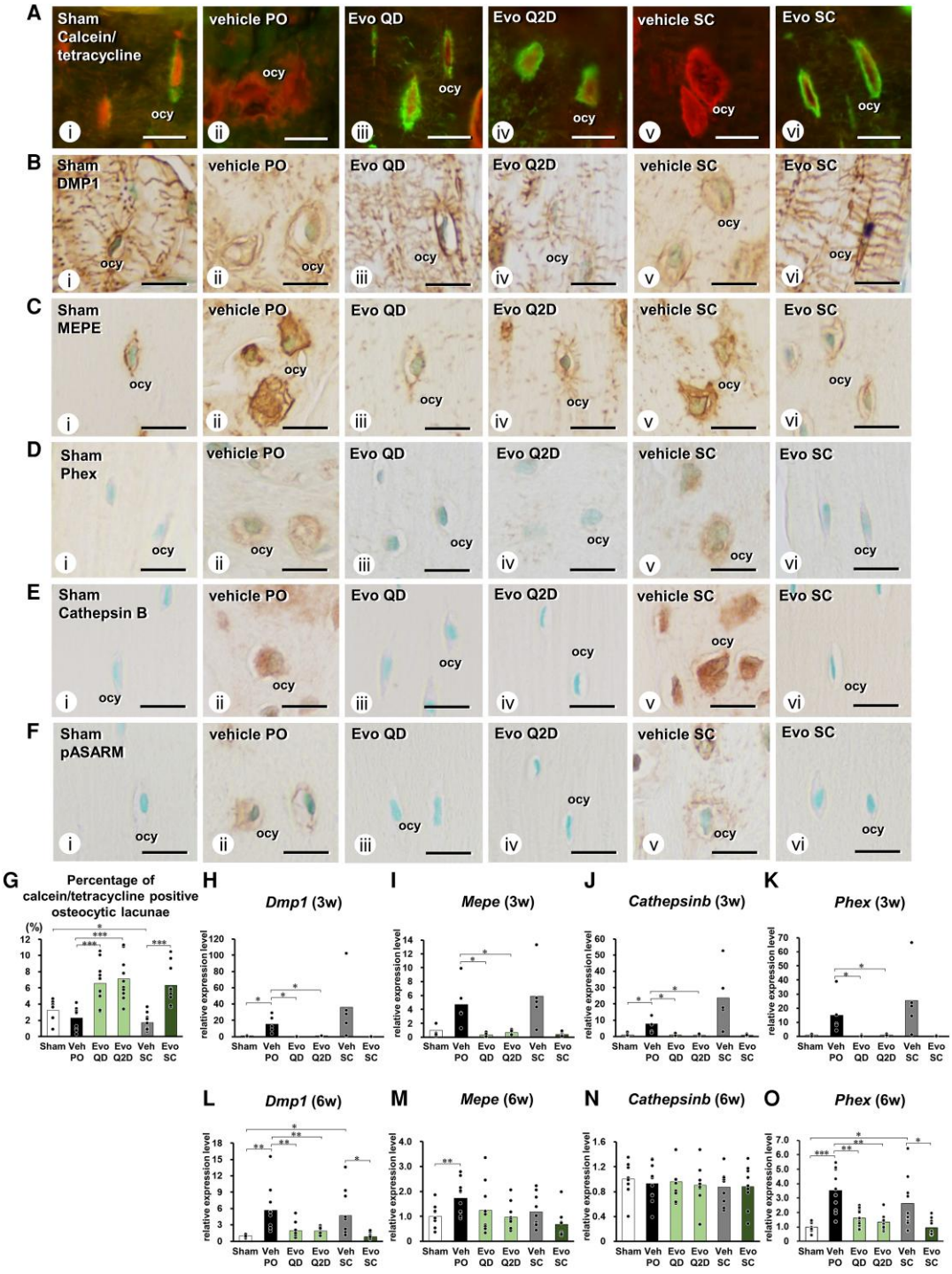

Figure 5. Mineralization and localization of Phex and phosphorylated ASARM peptides in the osteocytes of CKD-SHPT rats. (A) Calcein (green)/ tetracycline (yellow green) labels on the undecalcified sections. The vehicle group (ii, v) showed enlarged osteocytic lacunae without calcein/ tetracycline labeling, while the Evo groups (iii, iv, vi) demonstrated calcein/tetracycline-labeled lacunae. Scale bars, 10 μm. (B–F) Immunolocalization of Phex, DMP1, MEPE, cathepsin B, and pASARM in the femoral cortical bone after 6 weeks of evocalcet administration (n = 10; scale bars, 10 μm). (B) DMP1 immunoreactivity (brown) was detectable in the osteocytes of all groups. (C) The immunoreactivity of MEPE (brown) was intense in the osteocytes of the vehicle groups (ii, v). Immunoreactivities of (D) Phex, (E) cathepsin B, and (F) pASARM were seen in the osteocytes of the vehicle groups (ii, v). (G) Statistical analysis of the percentage of calcein/tetracycline-positive osteocytic lacunae after 6 weeks of evocalcet administration (n = 10 per group). The percentage of calcein/tetracycline-positive osteocytic lacunae significantly increased in the Evo groups compared with that in the vehicle group. (H-K) Quantitative PCR analyses of indicated genes in the femoral cortical bone after 3 weeks of evocalcet administration. (n = 5 per group). The expression levels of each gene increased in the vehicle group compared with those in the sham group; conversely, the expressions levels decreased in the Evo group compared with that in the vehicle group. (L–O) Quantitative PCR analyses of indicated genes in the whole femora after 6 weeks of evocalcet administration (n = 10 per group). Expression levels of *Dmp1* and *Phex* in the vehicle groups were significantly higher than those in the sham group and the Evo groups. Data are shown as the mean ± SE differences with $P < 0.05$ were considered significant different (see Methods). ***, $P < 0.001$; **, $P < 0.01$; *, $P < 0.05$.

Abbreviations: DMP1, dentin matrix protein 1; MEPE, matrix extracellular phosphoglycoprotein; ocy, osteocyte; pASARM, phosphorylated ASARM peptides.

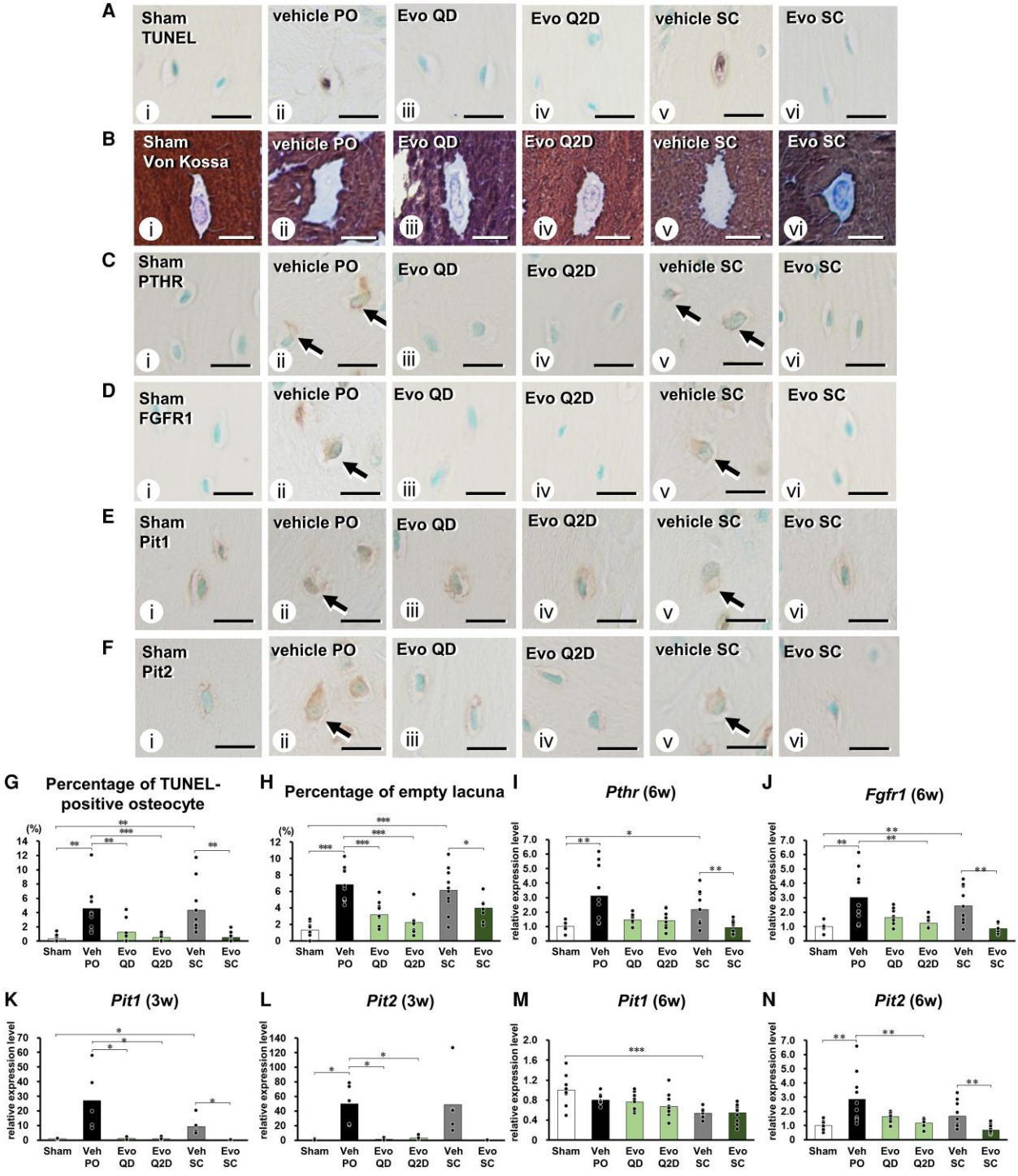

Figure 6. Osteocytic apoptosis, empty lacunae, and Pit1/Pit2, PTHR, and FGFR1 localization in the osteocytes of CKD-SHPT rats. (A, B) Osteocytic death at the endpoint (after 6 weeks of drug administration; scale bars, 10 μm). (A) Apoptotic osteocytes by TUNEL staining. (B) Empty lacunae by von Kossa staining. TUNEL-positive osteocytes and empty lacunae were observed in the vehicle groups (ii, v) but hardly detected in the Evo groups (iii, iv, vi). (C-F) Immunolocalization of (C) PTHR, (D) FGFR1, (E) Pit1, and (F) Pit2. Osteocytes of the vehicle groups (ii, v) exhibit PTHR and FGFR1 positivity (brown, arrows). Although the osteocytes in all groups show Pit1 immunopositivity (brown), Pit2 reactivity is relatively intense in the vehicle groups (ii, v). (G) Percentage of TUNEL-positive osteocytes (n = 10 per group). (H) Percentage of empty lacunae (n = 10 per group). The percentages of TUNEL-positive osteocytes and empty lacunae in the vehicle group significantly increased. (I, J) mRNA expression levels of (I) *Pthr* and (J) *Fgfr1* in the whole femora at the endpoint (n = 10 per group; scale bars, 10 μm). *Pthr* and *Fgfr1* expression levels significantly increased in the vehicle groups (ii, v) compared with those in the sham group (i). (K-N) Expression levels of (K, M) *Pit1* and (L, N) *Pit2* in the femoral cortical bone at the midpoint of the experimental period (n = 5 per group) and in the whole femora at the endpoint (n = 10 per group). *Pit1* and *Pit2* expression levels in the vehicle groups at the midpoint significantly increased compared with those in the sham group but decreased in the Evo groups. At the endpoint, *Pit2* expression levels were increased in the vehicle groups and decreased in the Evo groups. Data are shown as the mean ± SE; differences with $P < 0.05$ are considered significant (see Methods). ***, $P < 0.001$; **, $P < 0.01$; *, $P < 0.05$.

Abbreviations: FGFR1, fibroblast growth factor receptor 1; Pit1, sodium-dependent phosphate transporter 1; Pit2, sodium-dependent phosphate transporter 2; PTHR, PTH receptor; TUNEL, terminal deoxynucleotidyl transferase-mediated dUTP nick-end labeling.

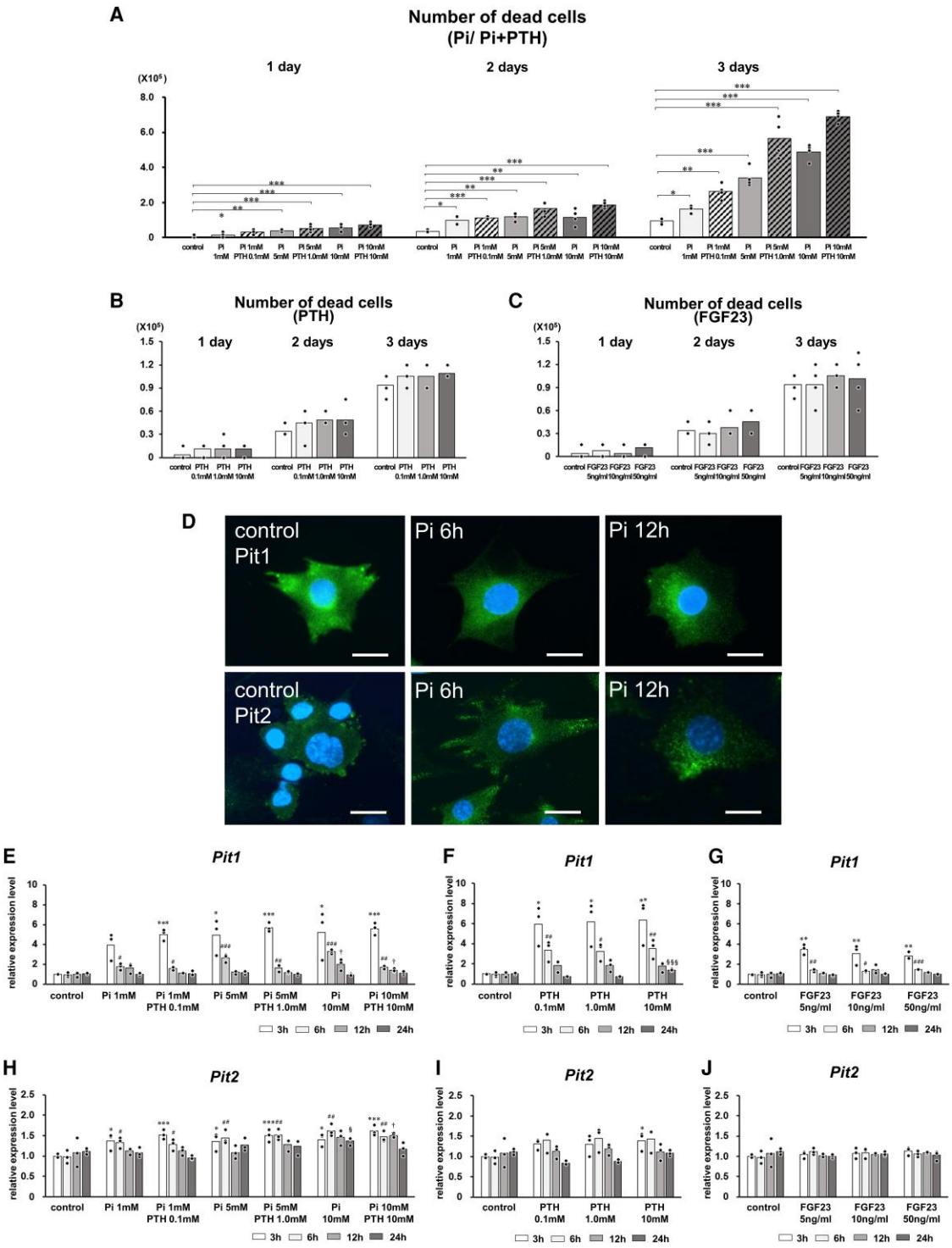

Figure 7. Effect of PTH and Pi on MLO-Y4 cell death. (A–C) Cell death levels in MLO-Y4 cells cultured with (A) Pi or the mixture of Pi and PTH (Pi + PTH); (B) PTH, and (C) FGF23 for 1 to 3 days (n = 4). Cell death levels in cells treated with Pi were much higher than those in controls in a dose and time-dependent manner. Cell death levels in cells treated with Pi + PTH were higher than those in the cells treated with Pi. Conversely, cell death levels in cells treated with PTH or FGF23 were similar to those in the control cells. ***, $P < 0.001$; **, $P < 0.01$; *, $P < 0.05$ (compared with control). (D) Localization of Pit1 and Pit2 (green) in MLO-Y4 cells after 6 and 12 hours of Pi treatment (n = 3; nuclei stained with DAPI). Pit1 and Pit2 immunoreactivities were localized around the cell membrane in the MLO-Y4 cells without Pi treatment. In Pi-treated MLO-Y4 cells, Pit1 and Pit2 immunoreactivities were observed in the granular structure inside the cells. (E-J) Expression levels of *Pit1* and *Pit2* in MLO-Y4 cells treated with indicated compounds for 3, 6, 12, and 24 hours (n = 3). Pit1 expression levels in MLO-Y4 cells increased significantly after 3 hours in all Pi, PTH, and FGF23 treatments; thereafter, the expression levels decreased with increased duration of treatment. *Pit1* expression levels were elevated more substantially by Pi or PTH treatment than by FGF23 treatment. *Pit2* expression in MLO-Y4 cells slightly increased when the cells were treated with Pi and PTH. The *Pit2* expression did not markedly change by FGF23 treatment. ***, $P < 0.001$; **, $P < 0.01$; *, $P < 0.05$ (compared with the 3-hour controls). ###, $P < 0.001$; ##, $P < 0.01$; #, $P < 0.05$ (compared with the 6-hour controls). †††, $P < 0.001$; ††, $P < 0.01$; †, $P < 0.05$ (compared with the 12-hour controls). §§§, $P < 0.001$; §§, $P < 0.01$; §, $P < 0.05$ (compared with the 24-hour controls). Data are shown as the mean ± SE; differences with $P <$ 0.05 were considered significant.

Abbreviations: FGF23, fibroblast growth factor 23; Pi, inorganic phosphate.

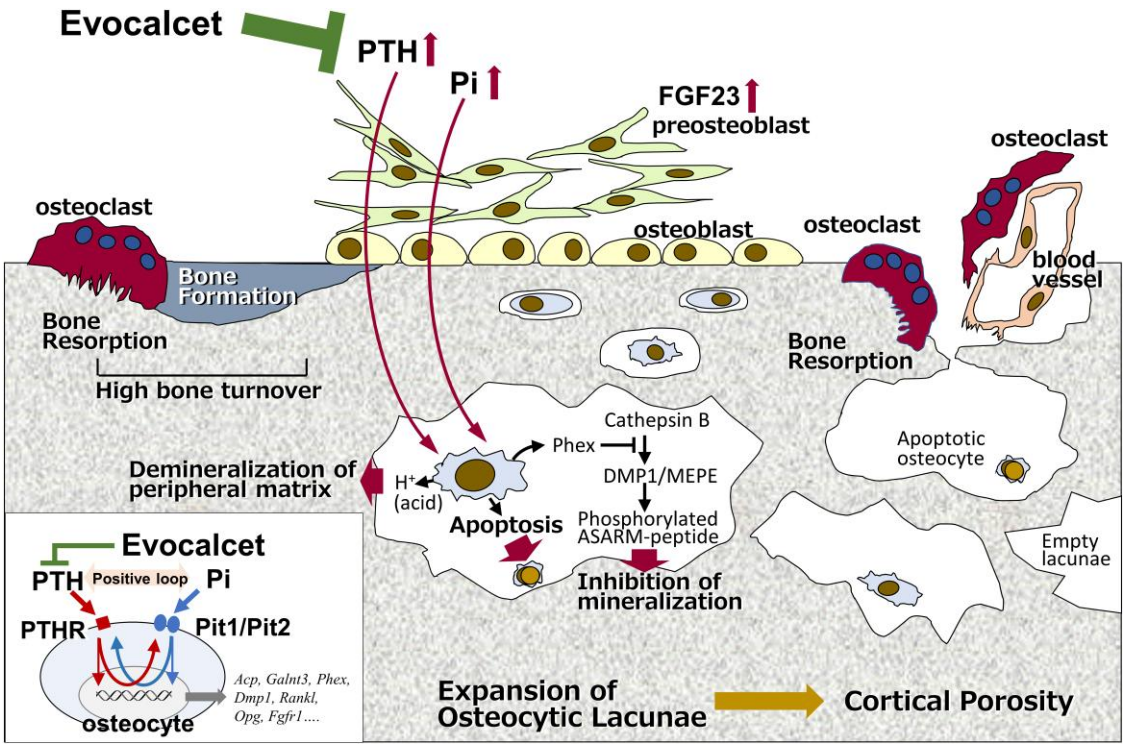

Figure 8. Schematic illustration of the cellular mechanism of cortical porosity and the inhibitory effect of evocalcet on SHPT model rats. Elevated serum PTH and Pi in CKD-SHPT induced osteocytic osteolysis, Phex/SIBLING-mediated inhibition of mineralization, and osteocytic death, which were the first steps of cortical porosity. PTH enhanced extracellular Pi sensing by stimulating Pit1 expression; PTH and Pi exacerbated cortical porosity in SHPT by enhancing their action toward each other. However, evocalcet, as a calcimimetic agent, prevented the PTH–Pi interaction and inhibited the enlargement of osteocytic lacunae and cortical porosity by decreasing the serum PTH concentration.

Abbreviations: Pi, inorganic phosphate; SHPT, secondary hyperparathyroidism.

cortical porosity in CKD-SHPT rats. CKD-SHPT rats showed broad demineralization around the osteocytes, little Ca deposition on the walls of the osteocytic lacunae, and increased osteocytic cell death, which constitute the initial step for the cortical porosity. However, evocalcet administration resulted in the prevention of broad demineralization, remineralization of osteocytic lacunae, and the attenuation of osteocytic cell death. Taken together, evocalcet seems to reduce bone fragility by not only attenuating bone turnover but also improving SHPT-driven cortical porosity (Fig. 8).

We assumed that the degree of cortical porosity in SHPT may be much more severe than that observed in osteoporotic treatment with PTH or teriparatide (32). In clinics, Nickolas et al have reported that the degree of cortical porosity in the tibia and radius increased by approximately 4.2% per 18 months in patients with CKD stages 2 to 5D with SHPT (33), whereas the cortical porosity rate in the PTH 1-34-treated osteoporotic patients increased by 1.1% in the tibia and 0.7% in the radius (34). Upon PTH administration into osteoclast-deficient mice, demineralization in the vicinity of osteocytes, ie, osteocytic osteolysis, becomes discernible (35), and subsequent remineralization is detected on the once-demineralized osteocytic lacunae (35–37). However, in CKD-SHPT rats examined here, bone minerals around the osteocytic lacunae were discharged, and imaging revealed that void spaces were connected to the enlarged adjacent osteocytic lacunae and some osteocytes exhibited apoptosis eventually featuring empty lacunae. Therefore, in a state of SHPT, osteocytic demineralization appeared to be markedly facilitated.

In addition, we conjecture that the Phex/SIBLING family might be involved in mineralization around the osteocytic lacunae in a SHPT environment. It seems possible that cathepsin B would cleave MEPE and DMP1 secreted by osteocytes (38–41) into ASARM peptides, which would be phosphorylated to suppress mineralization (42–44). Conversely, the formation of ASARM peptides could be inhibited by Phex produced by osteocytes (39, 44–46). Our study suggests the possibility that the phosphorylated ASARM peptide inhibited mineralization in osteocytic lacunae in the cortical bone of CKD-SHPT rats because the phosphorylated ASARM peptide was finally detected in the enlarged lacunae.

Our findings provided insights into the pathogenic mechanism of the severe cortical porosity, that is, the exacerbating interplay between PTH and Pi in osteocytic osteolysis, inhibition of mineralization, and osteocytic death. Given that Pi increased the *Pthr* expression in cultured osteocytes and their cell death in a concentration-dependent manner and that PTH increased the expression of *Pit1*, which may sense extracellular Pi, we hypothesize that PTH and Pi induce osteocytic cell death by increasing the expression of *Pit1* and *Pthr*, suggesting a PTH–Pi interaction. It is likely in particular that PTH and Pi may exacerbate cortical porosity in SHPT by enhancing their action toward each other in osteocytes in cortical bones. If so, the cortical porosity induced by SHPT bearing the elevated serum PTH and Pi could be much worse, compared with the osteocytic osteolysis merely induced by temporary PTH administration (32–37). Evocalcet, in contrast, may cut off the interplay of PTH and Pi actions to inhibit

the enlargement of osteocytic lacunae and cortical porosity by lowering the serum PTH levels.

The management of serum Pi appears important; serum Pi levels in the normal to high range increase the risk of fractures even in a state of good health, and serum Pi levels are an important risk factor for fractures in males (9, 10). Furthermore, elevated levels of serum Pi might gradually weaken the bone around the osteocytic network. Although evocalcet did not significantly reduce the serum Pi levels in CKD-SHPT rats in this study, it decreased not only serum PTH but also the serum Pi levels in patients undergoing dialysis (21). The discrepancy between this animal model and such patients was probably due to residual renal function in the partial nephrectomy model; since PTH reduces Pi reabsorption in the proximal tubule (47, 48), lowering PTH by evocalcet in this rat model might reduce Pi excretion because of a residual renal function. From the clinical viewpoint, evocalcet might efficiently reduce the serum levels of PTH and Pi in dialysis patients with SHPT to inhibit cortical porosity; therefore, further clinical data should be obtained.

The biological effect of Pi on bones is less clear than that of PTH. While human osteoblasts have been induced to undergo apoptosis by increasing extracellular Pi concentrations (49, 50), our work on CKD-SHPT rats demonstrated the presence of increased numbers of TUNEL-positive osteocytes and empty lacunae, which were considered to be consistent with previous reports. Although our in vitro experiments indicated that the number of dead MLO-Y4 cells did not increase in the FGF23- or PTH alone-treated groups, the number of dead cells increased significantly in the Pi administration group. In addition, the administration of PTH and Pi increased the number of dead MLO-Y4 cells compared with that in the group supplemented with Pi alone. These results suggested that, while highly concentrated Pi induced osteocytic death, PTH enhanced the action thereof.

The strength and new insights of our study is that CKD-SHPT may affect osteocytes by enlarging the demineralized peripheral areas of their lacunae, as well as by causing cell death. Our study suggests the possibly exacerbated effects of PTH and Pi on osteocytes in the CKD-SHPT state. Taken together, the bone abnormalities of CKD-SHPT have been attributed to accelerated bone turnover; however, this study provides a new insight on osteocytic cell death and demineralization surrounding the bone matrix. In addition, evocalcet, a new oral calcimimetic, ameliorated osteocytic abnormalities. In contrast, one of the weaknesses of this study is that CKD-SHPT was experimentally induced in growing young rats 17 weeks of age. Unlike in human CKD patients, the 7-week-old rats were suddenly 5/6 nephrectomized for 10 weeks. Therefore, we think that this study has the limitation of mimicking the long-lasting pathological states on bone turnover and bone quality, as could be seen in clinical CKD-SHPT in human patients. Although we have focused on CKD-MBD, it is possible that other factors, such as indoxyl sulfate, which induces uremia, as well as kidney failure-related humoral factors, such as fetuin-A, may also affect mineral metabolism (51–53). In addition, it is possible that evocalcet may affect not only parathyroid glands but also osteoblasts and osteocytes directly. It is necessary to examine these possibilities in the future.

In conclusion, the CKD rats in the present study developed SHPT, which resulted in increased serum PTH and Pi levels and severe cortical porosity. The elevated serum levels of PTH and Pi may have exacerbated cortical porosity in SHPT by enhancing their action toward each other. However, evocalcet, a calcimimetic, likely terminated the exacerbation by PTH–Pi interplay on the demineralization of osteocytic lacunae and cortical porosity by decreasing the serum PTH levels.

Acknowledgments

We would like to thank the following: Prof. Yuji Yoshiko and Dr. Tomoko Minamizaki (Hiroshima University) for kindly providing anti-phosphorylated ASARM peptide antibody (Bio-Rad AbD Serotec GmbH. Inc., Puchheim, Germany, and GeneFrontier Corp., Kashiwa, Japan); Mitsubishi Tanabe Pharma Corporation for providing evocalcet; Miki Murai and Misaki Kobayashi (Kyowa Kirin Co., Ltd.) for their assistance in the animal and tissue preparation; Kureha Special Laboratory Co., Ltd. for their assistance in bone histomorphometry analyses and mechanical (bone strength) test; and Rhelixa Co., Ltd. for their assistance in RNA sequencing analysis.

Funding

This study was partially supported by grants from the Japan Society for the Promotion of Science (21H03103 to N.A., 19K10040 and 22K09911 to T.H.) and partially supported by research funds from Kyowa Hakko Kirin Co., Ltd.

Author Contributions

T.H., S.T., T.K., and N.A. contributed to the conception and design of the research. T.H. was mainly in charge of this work, including histological sectioning, histochemical analyses, real time PCR, cell culture, and cell death measurement. T.Y. contributed to the experimental work, including paraffin sample preparation, micro-CT analyses, bone histomorphometry, and quantitative PCR. S.T. and M.S. contributed to animal preparation, including nephrectomy and feeding with a high phosphate diet, serum marker measurement, mechanical test, and statistical analyses. H.H. worked on histochemical analyses and bone histomorphometry. T.H. and S.T. wrote the initial draft of the manuscript. T.K. and N.A. participated in the discussion, editing, and formatting of the manuscript.

Disclosures

T.H., T.Y., H.H., and N.A. have nothing to declare. S.T., M.S., and T.K. are employees of Kyowa Kirin Co., Ltd.

Data Availability

The datasets generated and/or analyzed during the current study are not publicly available but are available from the corresponding author on reasonable request.

References

1. Joy MS, Karagiannis PC, Peyerl FW. Outcomes of secondary hyperparathyroidism in chronic kidney disease and the direct costs of treatment. *J Manag Care Pharm*. 2007;13(5):397-411. https://doi.org/10.18553/jmcp.2007.13.5.397
2. Saliba W, El-Haddad B. Secondary hyperparathyroidism: pathophysiology and treatment. *J Am Board Fam Med*. 2009;22(5):574-581. https://doi.org/10.3122/jabfm.2009.05.090026

3. Cunningham J, Locatelli F, Rodriguez M. Secondary hyperparathyroidism: pathogenesis, disease progression, and therapeutic options. *Clin J Am Soc Nephrol*. 2011;6(4):913-921. https://doi.org/10.2215/CJN.06040710
4. Go AS, Chertow GM, Fan D, McCulloch CE, Hsu CY. Chronic kidney disease and the risks of death, cardiovascular events, and hospitalization. *N Engl J Med*. 2004;351(13):1296-1305. https://doi.org/10.1056/NEJMoa041031
5. Reiss AB, Miyawaki N, Moon J, *et al*. CKD, arterial calcification, atherosclerosis and bone health: inter-relationships and controversies. *Atherosclerosis*. 2018;278:49-59. https://doi.org/10.1016/j.atherosclerosis.2018.08.046
6. Khairallah P, Nickolas TL. Management of osteoporosis in CKD. *Clin J Am Soc Nephrol*. 2018;13(6):962-969. https://doi.org/10.2215/CJN.11031017
7. Mazzaferro S, Pasquali M. Direct bone effects of calcimimetics in chronic kidney disease? *Kidney Int*. 2019;95(5):1012-1014. https://doi.org/10.1016/j.kint.2019.01.045
8. Tsuchiya K, Akihisa T. The importance of phosphate control in chronic kidney disease. *Nutrients*. 2021;13(5):1670. https://doi.org/10.3390/nu13051670
9. Campos-Obando N, Koek WNH, Hooker ER, *et al*. Serum phosphate is associated with fracture risk: the Rotterdam study and MrOS. *J Bone Miner Res*. 2017;32(6):1182-1193. https://doi.org/10.1002/jbmr.3094
10. Fusaro M, Holden R, Lok C, *et al*. Phosphate and bone fracture risk in chronic kidney disease patients. *Nephrol Dial Transplant*. 2021;36(3):405-412. https://doi.org/10.1093/ndt/gfz196
11. Mizobuchi M, Ogata H, Koiwa F. Secondary hyperparathyroidism: pathogenesis and latest treatment. *Ther Apher Dial*. 2019;23(4):309-318. https://doi.org/10.1111/1744-9987.12772
12. Komaba H, Ketteler M, Cunningham J, Fukagawa M. Old and new drugs for the management of bone disorders in CKD. *Calcif Tissue Int*. 2021;108(4):486-495. https://doi.org/10.1007/s00223-020-00788-y
13. de Freitas PHL, Li M, Ninomiya T, *et al*. Intermittent PTH administration stimulates pre-osteoblastic proliferation without leading to enhanced bone formation in osteoclast-less c-fos(-/-) mice. *J Bone Miner Res*. 2009;24(9):1586-1597. https://doi.org/10.1359/jbmr.090413
14. Yamamoto T, Hasegawa T, Sasaki M, *et al*. Frequency of teriparatide administration affects the histological pattern of bone formation in young adult male mice. *Endocrinology*. 2016;157(7):2604-2620. https://doi.org/10.1210/en.2015-2028
15. Behets GJ, Spasovski G, Sterling LR, *et al*. Bone histomorphometry before and after long-term treatment with cinacalcet in dialysis patients with secondary hyperparathyroidism. *Kidney Int*. 2015;87(4): 846-856. https://doi.org/10.1038/ki.2014.349
16. Moe SM, Abdalla S, Chertow GM, *et al*. Effects of cinacalcet on fracture events in patients receiving hemodialysis: the EVOLVE trial. *J Am Soc Nephrol*. 2015;26(6):1466-1475. https://doi.org/10.1681/ASN.2014040414
17. Akizawa T, Ikejiri K, Kondo Y, Endo Y, Fukagawa M. Evocalcet: a new oral calcimimetic for dialysis patients with secondary hyperparathyroidism. *Ther Apher Dial*. 2020;24(3):248-257. https://doi.org/10.1111/1744-9987.13434
18. Hamano N, Endo Y, Kawata T, Fukagawa M. Development of evocalcet for unmet needs among calcimimetic agents. *Expert Rev Endocrinol Metab*. 2020;15(5):299-310. https://doi.org/10.1080/17446651.2020.1780911
19. Miyazaki H, Ikeda Y, Sakurai O, *et al*. Discovery of evocalcet, a next-generation calcium-sensing receptor agonist for the treatment of hyperparathyroidism. *Bioorg Med Chem Lett*. 2018;28(11):2055-2060. https://doi.org/10.1016/j.bmcl.2018.04.055
20. Kawata T, Tokunaga S, Murai M, *et al*. A novel calcimimetic agent, evocalcet (MT-4580/KHK7580), suppresses the parathyroid cell function with little effect on the gastrointestinal tract or CYP isozymes in vivo and in vitro. *PLoS One*. 2018;13(4):e0195316.https://doi.org/10.1371/journal.pone.0195316
21. Fukagawa M, Shimazaki R, Akizawa T; Evocalcet Study Group. Head-to-head comparison of the new calcimimetic agent evocalcet with cinacalcet in Japanese hemodialysis patients with secondary hyperparathyroidism. *Kidney Int*. 2018;94(4):818-825. https://doi.org/ 10.1016/j.kint.2018.05.013
22. Ishii H, Wada M, Furuya Y, Nagano N, Nemeth EF, Fox J. Daily intermittent decreases in serum levels of parathyroid hormone have an anabolic-like action on the bones of uremic rats with low-turnover bone and osteomalacia. *Bone*. 2000;26(2):175-182. https://doi.org/ 10.1016/s8756-3282(99)00263-x
23. Parfitt AM, Drezner MK, Glorieux FH, *et al*. Bone histomorphometry: standardization of nomenclature, symbols, and units. Report of the ASBMR Histomorphometry Nomenclature Committee. *J Bone Miner Res*. 1987;2(6):595-610. https://doi.org/ 10.1002/jbmr.5650020617
24. Ammann P, Zacchetti G, Gasser JA, Lavet C, Rizzoli R. Protein malnutrition attenuates bone anabolic response to PTH in female rats. *Endocrinology*. 2015;156(2):419-428. https://doi.org/10.1210/en.2014-1033
25. Charoenphandhu N, Suntornsaratoon P, Krishnamra N, *et al*. Fibroblast growth factor-21 restores insulin sensitivity but induces aberrant bone microstructure in obese insulin-resistant rats. *J Bone Miner Metab*. 2017;35(2):142-149. https://doi.org/10.1007/s00774-016-0745-z
26. Oda K, Amaya Y, Fukushi-Irié M, *et al*. A general method for rapid purification of soluble versions of glycosylphosphatidylinositol-anchored proteins expressed in insect cells: an application for human tissue-nonspecific alkaline phosphatase. *J Biochem*. 1999;126(4):694-699. https://doi.org/10.1093/oxfordjournals.jbchem.a022505
27. Minamizaki T, Sakurai K, Hayashi I, *et al*. Active sites of human MEPE-ASARM regulating bone matrix mineralization. *Mol Cell Endocrinol*. 2020;517:110931. https://doi.org/10.1016/j.mce.2020.110931
28. Hasegawa T, Miyamoto-Takasaki Y, Abe M, *et al*. Histochemical examination on principal collagen fibers in periodontal ligaments of ascorbic acid-deficient ODS-od/od rats. *Microscopy*. 2019;68(5):349-358. https://doi.org/10.1093/jmicro/dfz021
29. Hasegawa T, Yamamoto T, Sakai S, *et al*. Histological effects of the combined administration of eldecalcitol and a parathyroid hormone in the metaphyseal trabeculae of ovariectomized rats. *J Histochem Cytochem*. 2019;67(3):169-184. https://doi.org/ 10.1369/0022155418806865
30. Hasegawa T, Tokunaga S, Yamamoto T, *et al*. Evocalcet rescues secondary hyperparathyroidism-driven cortical porosity in chronic kidney disease male rats. *Endocrinology* Published online. January 2023. https://doi.org/10.6084/m9.figshare.22067381
31. Kato Y, Windle JJ, Koop BA, Mundy GR, Bonewald LF. Establishment of an osteocyte-like cell line, MLO-Y4. *J Bone Miner Res*. 1997;12(12):2014-2023. https://doi.org/ 10.1359/jbmr.1997.12.12.2014
32. Lotinun S, Evans GL, Bronk JT, *et al*. Continuous parathyroid hormone induces cortical porosity in the rat: effects on bone turnover and mechanical properties. *J Bone Miner Res*. 2004;19(7):1165-1171. https://doi.org/10.1359/JBMR.040404
33. Nickolas TL, Stein EM, Dworakowski E, *et al*. Rapid cortical bone loss in patients with chronic kidney disease. *J Bone Miner Res*. 2013;28(8):1811-1820. https://doi.org/10.1002/jbmr.1916
34. Hansen S, Hauge EM, Beck Jensen JE, Brixen K. Differing effects of PTH 1–34, PTH 1–84, and zoledronic acid on bone microarchitecture and estimated strength in postmenopausal women with osteoporosis: an 18-month open-labeled observational study using HR-pQCT. *J Bone Miner Res*. 2013;28(4):736-745. https://doi.org/10.1002/jbmr.1784
35. Hongo H, Hasegawa T, Saito M, *et al*. Osteocytic osteolysis in PTH-treated wild-type and *Rankl*$^{-/-}$ mice examined by transmission electron microscopy, atomic force microscopy, and isotope microscopy. *J Histochem Cytochem*. 2020;68(10):651-668. https://doi.org/10.1369/0022155420961375

36. Bélanger LF. Osteocytic osteolysis. *Calcif Tissue Res*. 1969;4(1):1-12. https://doi.org/10.1007/BF02279101
37. Qing H, Ardeshirpour L, Pajevic PD, *et al*. Demonstration of osteocytic perilacunar/canalicular remodeling in mice during lactation. *J Bone Miner Res*. 2012;27(5):1018-1029. https://doi.org/10.1002/jbmr.1567
38. Toyosawa S, Shintani S, Fujiwara T, *et al*. Dentin matrix protein 1 is predominantly expressed in chicken and rat osteocytes but not in osteoblasts. *J Bone Miner Res*. 2001;16(11):2017-2026. https://doi.org/10.1359/jbmr.2001.16.11.2017
39. Thompson DL, Sabbagh Y, Tenenhouse HS, *et al*. Ontogeny of Phex/PHEX protein expression in mouse embryo and subcellular localization in osteoblasts. *J Bone Miner Res*. 2002;17(2):311-320. https://doi.org/10.1359/jbmr.2002.17.2.311
40. Nampei A, Hashimoto J, Hayashida K, *et al*. Matrix extracellular phosphoglycoprotein (MEPE) is highly expressed in osteocytes in human bone. *J Bone Miner Metab*. 2004;22(3):176-184. https://doi.org/10.1007/s00774-003-0468-9
41. Feng JQ, Ward LM, Liu S, *et al*. Loss of DMP1 causes rickets and osteomalacia and identifies a role for osteocytes in mineral metabolism. *Nat Genet*. 2006;38(11):1310-1315. https://doi.org/10.1038/ng1905
42. Rowe PS, Garrett IR, Schwarz PM, *et al*. Surface plasmon resonance (SPR) confirms that MEPE binds to PHEX via the MEPE-ASARM motif: a model for impaired mineralization in X-linked rickets (HYP). *Bone*. 2005;36(1):33-46. https://doi.org/10.1016/j.bone.2004.09.015
43. Boskey AL, Chiang P, Fermanis A, *et al*. MEPE's diverse effects on mineralization. *Calcif Tissue Int*. 2010;86(1):42-46. https://doi.org/10.1007/s00223-009-9313-z
44. Staines KA, MacRae VE, Farquharson C. The importance of the SIBLING family of proteins on skeletal mineralisation and bone remodelling. *J Endocrinol*. 2012;21(3):241-255. https://doi.org/10.1530/JOE-12-0143
45. Guo R, Rowe PS, Liu S, Simpson LG, Xiao ZS, Quarles LD. Inhibition of MEPE cleavage by Phex. *Biochem Biophys Res Commun*. 2002;297(1):38-45. https://doi.org/10.1016/s0006-291x(02)02125-3
46. Yuan B, Takaiwa M, Clemens TL, *et al*. Aberrant Phex function in osteoblasts and osteocytes alone underlies murine X-linked hypophosphatemia. *J Clin Invest*. 2008;118(2):722-734. https://doi.org/10.1172/JCI32702
47. Bergwitz C, Juppner H. Regulation of phosphate homeostasis by PTH, vitamin D, and FGF23. *Annu Rev Med*. 2010;61(1):91-104. https://doi.org/10.1146/annurev.med.051308.111339
48. Lederer E. Regulation of serum phosphate. *J Physiol*. 2014;592-(18):3985-3995. https://doi.org/10.1113/jphysiol.2014.273979
49. Meleti Z, Shapiro IM, Adams CS. Inorganic phosphate induces apoptosis of osteoblast-like cells in culture. *Bone*. 2000;27(3):359-366. https://doi.org/10.1016/s8756-3282(00)00346-x
50. Adams CS, Mansfield K, Perlot RL, Shapiro IM. Matrix regulation of skeletal cell apoptosis. Role of calcium and phosphate ions. *J Biol Chem*. 2001;276(23):20316-20322. https://doi.org/10.1074/jbc.M006492200
51. Messa P, Alberti L, Como G, *et al*. Calcimimetic increases osteoprotegerin and decreases fetuin-A levels in dialysis patients. *Nephrol Dial Transplant*. 2007;22(9):2724-2725. https://doi.org/10.1093/ndt/gfm312
52. Mattinzoli D, Rastaldi MP, Ikehata M, *et al*. FGF23-regulated production of fetuin-A (AHSG) in osteocytes. *Bone*. 2016;83:35-47. https://doi.org/10.1016/j.bone.2015.10.008
53. Smith ER, Hewitson TD, Jahnen-Dechent W. Calciprotein particles: mineral behaving badly? *Curr Opin Nephrol Hypertens*. 2020;29(4):378-386. https://doi.org/10.1097/MNH.0000000000000609